NDT&E International 108 (2019) 102172

Contents lists available at ScienceDirect

NDT and E International

journal homepage: http://www.elsevier.com/locate/ndteint

Thermal damage assessment of metallic plates using a nonlinear electromagnetic acoustic resonance technique

Weibin Li [a], Chang Jiang [a], Mingxi Deng [b,*]

[a] School of Aerospace Engineering, Xiamen University, 422, South Siming Road, Xiamen, 361005, China
[b] College of Aerospace Engineering, Chongqing University, Chongqing, 400044, China

ARTICLE INFO

Keywords:
Contactless
Electromagnetic acoustic resonance (EMAR)
Thermal damage
Higher harmonic generation

ABSTRACT

Low efficiency of energy transition is generally considered to be the only weakness of electromagnetic ultrasonic transducers (EMATs). Electromagnetic acoustic resonance (EMAR) technique has been successfully used to overcome this disadvantage with a combination of the EMATs with the ultrasonic resonant method. In this paper, a nonlinear EMAR technique has been proposed to evaluate the thermal damage of metallic materials, which combines the feature of EMAR with the merit of higher harmonic generation that provides an effective indicator to material damage. The use of contactless EMATs can isolate the material nonlinearity and maintain the coupling condition consistently on measurements of higher harmonics generated. EMAR provides high enough signal magnitude for higher harmonic generated. An experimental scheme is proposed and applied to assess the thermal damage in aluminum and nickel plates. In addition, conventional EMAR techniques based on the measure of shear wave velocity and attenuation within a certain frequency range, are also carried out for the specimens. The experimental results show a monotonic relationship between the normalized amplitude of higher harmonic generated and the artificial thermal loading time, while no stable trends are observed by conventional linear EMAR approaches. The results in this paper indicate that nonlinear EMAR technique proposed can be used to assess the thermal damage in both nonferromagnetic and ferromagnetic materials, with improved reliability and sensitivity over linear one.

1. Introduction

The use of ultrasonic waves has been widely applied for flaw detection and material characterization nondestructively. However, the accuracy of contact ultrasonic methods is generally affected by the coupling condition between specimens and ultrasonic transducers. In addition, some applications of ultrasonic testing under certain circumstances such as monitoring or assessment of components and structures in service of high temperature, require no coupling media and no surface preparations [1–4]. Thus, non-contacting ultrasonic measurements have drawn increasing concern for their capacity to conduct rapid and reliable in-situ continuous characterization and online monitoring [5,6]. Electromagnetic acoustic transducer (EMAT) is the contactless transducer for ultrasonic nondestructive testing, by which an effective ultrasonic measurement can be realized through a relatively easy and low-cost way [7]. The use of EMAT for ultrasonic testing plays an important role in the nondestructive testing (NDT) field, with the advantages of comparatively better reliability and temperature compatibility [8,9].

However, the particularly low efficiency of energy transition for EMATs typically leads to a low signal-to-noise ratio (SNR) compared to piezoelectric transducers [10,11]. To overcome this drawback, numerous efforts have been made to increase the SNR [12]. Electromagnetic acoustic resonance (EMAR) method is a combination of EMATs and ultrasonic resonance spectrum analysis for electromagnetic ultrasonic testing. The resonance ultrasound spectroscopy (RUS) is an established methodology for material characterization by many researchers [13–16], which generally involves piezoelectric transducers that cannot endure high temperature testing environment. Contacting piezoelectric transducers can be replaced by EMATs to realize higher accuracy and workability of ultrasonic testing. Thus, EMAR has been taken as an effective means to increase the SNR, with the significant potential of enhancing the received signal by superimposing multi-ultrasonic waves coherently. Kawashima et al. presented a unified theory of the resonant electromagnetic excitation and detection of ultrasonic waves travelling in the through-thickness direction in

* Corresponding author.
E-mail address: dengmx65@yahoo.com (M. Deng).

https://doi.org/10.1016/j.ndteint.2019.102172
Received 14 June 2019; Received in revised form 26 August 2019; Accepted 23 September 2019
Available online 25 September 2019

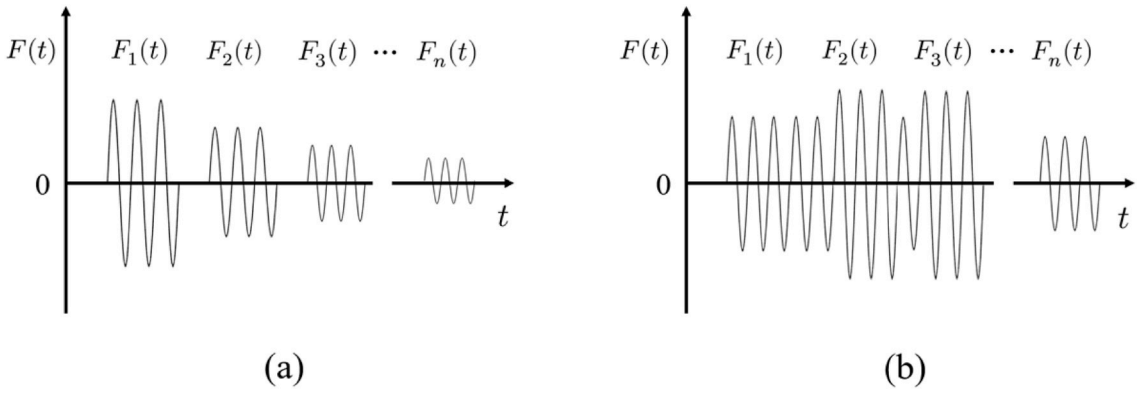

Fig. 1. Time-domain signal with multiple echoes, (a) three-cycle pulse input, (b) constructive interference of eight-cycle pulse input.

conducting sheets [17]. Hirao et al. conducted an experiment on the acoustic resonance spectrometer for evaluating the attenuation characteristics and grain size of polycrystalline metals [18]. Bin Wang et al. detected the mean size of DP590 steel plate using a modified approach combined with EMAR technique which reduced the relative errors [19]. It has been shown that the EMAR technique is an effective non-contact means for material characterization and defect detection due to its high SNR [20].

Another promising technique for material characterization is nonlinear ultrasonic measurements based on higher harmonic generation [21–23]. One of the typical nonlinear ultrasonic responses is the higher harmonic generation induced by waveform distortion of primary wave propagation [24,25]. Recently, higher harmonic generation is widely used to characterize micro-cracks, material degradation, and micro-structural change at early stage [26–31]. However, reliability of higher harmonic measurement in a contact way is generally suffered by the in-consistency of coupling condition and couplant effect [32]. Although EMATs can be used to maintain the coupling condition consistently owing to its non-contacting feature, higher harmonic could still be absent in the received signal due to the low efficiency of transition.

In this paper, a nonlinear EMAR technique is proposed based on the measurement of higher (third) harmonic generated by shear waves excited with EMATs, which combines the feature of EMAR with the merit of higher harmonic generation that provides an effective means to material characterization. Coherent superposition of echo signals produces highly magnified amplitude of higher harmonics. The use of contactless EMATs can isolate the material nonlinearity and minimize the coupling effect on the measure of third harmonic generated. EMAR provides high enough signal amplitude in the material for inducing third harmonics. The proposed approach was applied to the evaluation of thermal damage in ferromagnetic and non-ferromagnetic metals. In addition, conventional linear acoustic parameters of shear wave velocity and attenuation (represented by the total amplitude of resonance peaks within a certain frequency range) measured by the EMAR method were also conducted in the specimens. The sensitivity comparison of linear and nonlinear EMAR techniques is discussed for the assessment of thermal loadings in specimens.

2. Theoretical fundamentals

2.1. Resonance ultrasound spectrum

The principle of EMAR technique could be understood by considering a simple through-thickness resonance example in which the electromagnetic ultrasonic transmitter and receiver are placed on the opposite sides of a metal plate. When the excited sinusoidal burst wave propagates through the plate, a series of pulse-echo signals denoted by $F_1(t)$, $F_2(t)$, …, $F_n(t)$ will be measured, which superpose each other to form the received signal denoted by $F(t)$. Fig. 1 shows the examples of time-domain signals of the above through-thickness resonance example.

Formally we could use the trigonometric functions to express the $F_1(t)$, $F_2(t)$, …, $F_n(t)$ as follows

$$\begin{cases} F_1(t) = A_1(t)sin(2\pi ft + \phi_1) \\ F_2(t) = A_2(t)sin(2\pi ft + \phi_2) \\ \cdots \\ F_n(t) = A_n(t)sin(2\pi ft + \phi_n) \\ \phi_i = \phi_1 + (i-1)\cdot 2\pi ft\cdot 2d/c_s, \quad i = 1, 2, ..., n \end{cases} \tag{1}$$

where $A_i(t)$ is a modulation term, which defines the width, amplitude and shape of the received signal $F_i(t)$, f denotes the driving frequency of the excited input signal, d is the thickness of the specimen, c_s is the acoustic wave velocity, and ϕ_i is the phase of each echo.

The total received signal $F(t)$ consists all the pulse-echo signals, which can be given as [33,34].

$$\begin{aligned} F(t) &= \sum_{i=1}^{n} F_i(t) \\ &= \sum_{i=1}^{n} A_i(t)sin(2\pi ft + \phi_i) \\ &= A(t)sin(2\pi ft + \phi) \end{aligned} \tag{2}$$

It is known that EMATs can receive relatively more echoes due to its non-contact feature. The superheterodyne method can be utilized to process the $F(t)$ into two perpendicular components S_1 and S_2, given by Refs. [33,34].

$$\begin{aligned} S_1 &= R\sum_{i=1}^{n} \int_{t_1}^{t_2} A_i(t)dt\cdot cos\phi_i \\ S_2 &= R\sum_{i=1}^{n} \int_{t_1}^{t_2} A_i(t)dt\cdot sin\phi_i \end{aligned} \tag{3}$$

where R is a proportional coefficient and (t_1, t_2) is the gate length in the time domain of $F(t)$. The expression of integral amplitude $\int_{t_1}^{t_2} A_i(t)dt$ could be reckoned as the amplitude of the carrier signal of $F_i(t)$. Considering that the calculated integral amplitude of $F(t)$ varies with the phases of each received echo, the signal $F_i(t)$ in Eq. (2) are supposed to

Table 1
Chemical composition of the aluminum plate (weight %).

Al	Si	Fe	Cu	Mn	Mg	Zn	V
≥99.7	<0.10	<0.20	<0.04	<0.03	<0.03	<0.04	<0.03

Table 2
Chemical composition of the nickel plate (weight %).

Ni	Cu	Si	Mn	C	Mg	S	Fe
≥99.5	<0.06	<0.10	<0.05	<0.10	<0.10	<0.05	<0.10

Table 3
Thickness and disposal information of the aluminum plates and nickel plates.

No.	#A0	#A1	#A2	#A3	#A4	#A5	#B0	#B1	#B2	#B3	#B4	#B5
Material	Al	Al	Al	Al	Al	Al	Ni	Ni	Ni	Ni	Ni	Ni
Thickness (mm)	1.98	1.96	1.96	1.95	1.93	1.95	2.04	2.04	2.02	2.03	2.06	2.04
Heating time (min)	None	10	20	30	40	50	None	10	20	30	40	50

match the same phase with each other to reach the maximum magnitude of the received signal, conforming to the following equation [35].

$$\begin{aligned} \phi_i &= \phi_1 + (i-1)\cdot k\cdot 2\pi, \quad i = 1, 2, \ldots \\ k &= f\cdot 2d/c_s, \quad k \in Z \end{aligned} \tag{4}$$

where k in an integer. The correlation of the acoustic velocity c_s and the resonant frequency f_j can be given by the following equation

$$f_j = j\cdot\frac{c_s}{2d}, \quad j = 1, 2, \ldots \tag{5}$$

Consequently, by setting the length of integrator gate and frequency scanning range, the resonance frequency spectrum of the plate can be obtained. In addition, it should be noted that the resonance frequency spectrum remains measurable whether the ultrasonic echoes interfere with each other or not. Based on the above analysis, a damaged specimen whose elastic constants are supposed to be different from those of intact one, which generally result in the variations of acoustic velocity and attenuation manifested in the measured resonance spectra.

2.2. Nonlinear EMAR technique

Generally, one of the typical nonlinear ultrasonic phenomena is the generation of higher harmonics, i.e., the formation of harmonics double or triple the frequency of the primary (fundamental) ultrasonic wave, caused by the waveform distortion of time-domain signal propagating in the specimen with material nonlinearity. In this investigation, ultrasonic shear waves generated and detected by EMATs are employed for the nonlinear EMAR testing. The distinguishing feature of nonlinearity in shear waves is that it is primarily cubic rather than quadratic [36]. As described previously [37], a primary shear wave can only generate a second-order longitudinal wave, and no generation of second-order shear component. Consequently, the quadratic nonlinearity for shear wave propagation is negligible. The effect of third-harmonic generation of shear wave propagation is induced by the third-order self-interaction of the primary shear wave, generating the corresponding third harmonic shear wave which satisfies phase matching with the primary shear wave.

To conduct the nonlinear EMAR test, we have to measure the resonance frequency spectrum firstly, which can be obtained by sweeping the input frequency. Peak height of a suitable resonance frequency (f_r) is taken as the primary wave amplitude (A_1). Then, the EAMT is driven at one third of the resonance frequency (i.e. $f_r/3$) with the input power unchanged. It should be note that the driving frequency at $f_r/3$ does not satisfy the resonance condition. Thus, the primary wave amplitude ($\tilde{A}_1$) is not measurable [35]. However, the third harmonic at f_r, generated by primary shear wave at $f_r/3$ in the specimen, satisfies the resonance condition and remains with a measurable amplitude (A_3). Ultimately, the interaction of primary shear wave with the material nonlinearity generates the higher (third) harmonic whose magnitude is relatively obvious under the resonant circumstance. Normalization of A_3 versus A_1 at the resonance frequency (f_r) can be used to remove the influence of lifting off, frequency dependence of the transfer efficiency and other anomalies. It is expected that the damage state of the specimen can effectively be characterized using the normalized third-harmonic amplitude (expressed as A_3/A_1), which combines the feature of EMAR with the advantage of higher harmonic generation.

3. Experiments

3.1. Samples

It is well known that EMAT can be used to generate ultrasonic shear waves in metallic materials by the Lorenz force and/or the magnetostrictive effect, hence both the ferromagnetic and non-ferromagnetic materials are chosen to verify the validity of the nonlinear EMAR technique proposed. In this investigation, non-ferromagnetic aluminum plates and ferromagnetic nickel plates with rectangular shape are commercially provided by the same supplier. The chemical compositions of the two materials are presented in Tables 1 and 2. Five aluminum specimens and five nickel specimens were subjected to thermal loading in vacuum with different times at the temperature of 250 °C and 660 °C, respectively. The details of the thermal processes are presented in Table 3. The selected heating temperatures are the corresponding annealing temperatures for the materials. It is well known that grain recrystallization occurs and grain size changes during annealing process [38–41]. It is convinced that the change of material microstructure will affect the ultrasonic wave propagation in the tested specimens. Measurements were conducted when the specimens were cooled to room temperature. Since the following measurements were not related to in-situ testing of one sample, the thickness information of all the specimens were measured for the calculation of shear wave velocities.

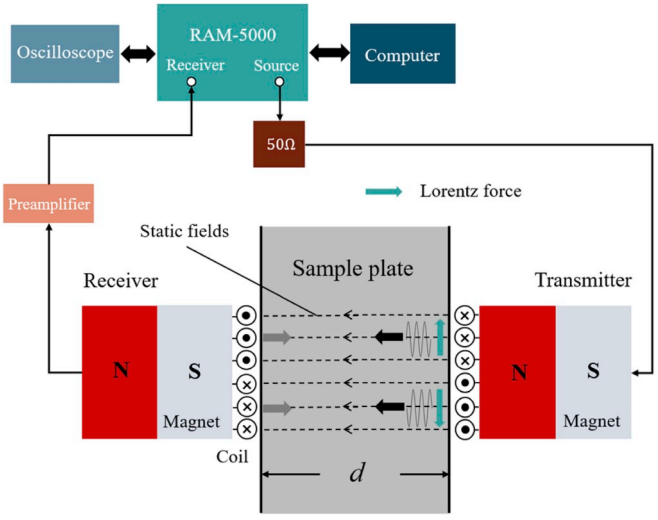

Fig. 2. Schematic of the EMAR measurement system and mechanism of the shear wave EMATs.

3.2. Transducers & experimental setup

The transducers employed in this investigation are EMATs, which are used to generate and measure the ultrasonic shear waves. The diameters of the cylindrical EMATs are 20 mm and the copper wires bind together closely to form the coils (1.0 mm×11 circles). The region in which the coils and permanent magnets overlap is the effective area to generate/measure the ultrasonic shear waves. The frequency bandwidths of the EMATs are from 1.0 MHz to 10 MHz. Fig. 2 shows the mechanism of shear wave generation by EMATs and the experimental setup. The cylindrical permanent magnets and spiral coil elements provide the biasing and dynamic magnetic fields to induce eddy currents in the metal surface. Radial ultrasonic shear waves propagating in the specimen can be generated by varying Lorentz force and/or magnetostrictive force in the specimen. Since the energy conversion efficiency of EMATs is rather lower than piezoelectric transducers, a pre-amplifier is connected to the experimental system. The measurements based on linear and nonlinear EMARs are conducted through the ultrasonic RAM-5000-SNAP system, which is able to generate enough power for signal excitations. The RF pulse voltage level and the gated amplifier are used to change the magnitude of the ultrasonic synthesizer source, and the integrator gate delay of the superheterodyne phase sensitive detector is used to control the width of measured signals in the time domain.

4. Results & discussions

4.1. Linear EMAR measurements

According to the theoretical analysis in Section 2, in the case of that the burst width of the exciting signal is less than the round-trip time ($2d/c_s$), the ultrasonic echoes propagating in materials will not overlap with each other as shown in Fig. 3(a). It has been confirmed that the resonance frequency spectrum can be measured whether the time-domain signals overlap coherently with each other or not. However, to enhance the shear wave signal received by the EMAT, the burst length of input signal should be long enough to result in coherent superposition of these echoes. As shown in Fig. 3(b), there is a larger particle vibration displacement in the tested material, which corresponds to greater amplitudes of the ultrasonic signals, at the condition of that the echoes are in phase with each other simultaneously.

In this work, continuous sinusoidal pulse signal of 20 cycles was generated and conducted to the EMAT. The integrator gate width was set to be 50 μs while the gain value of the receiver was set to be 70 dB, and the resonance frequency spectra of the aluminum plates were measured as presented in Fig. 4 by sweeping the frequency of RF burst signal from 1.0 to 10 MHz with the exact same instrument parameters. Similar measurement operation was applied to the nickel plates while the integrator gate width was set to be 30 μs. Owing to the relatively higher amplitude of measured signal in the ferromagnetic material, the gain was set to be 40 dB. As shown in Fig. 5, the resonance frequency spectra

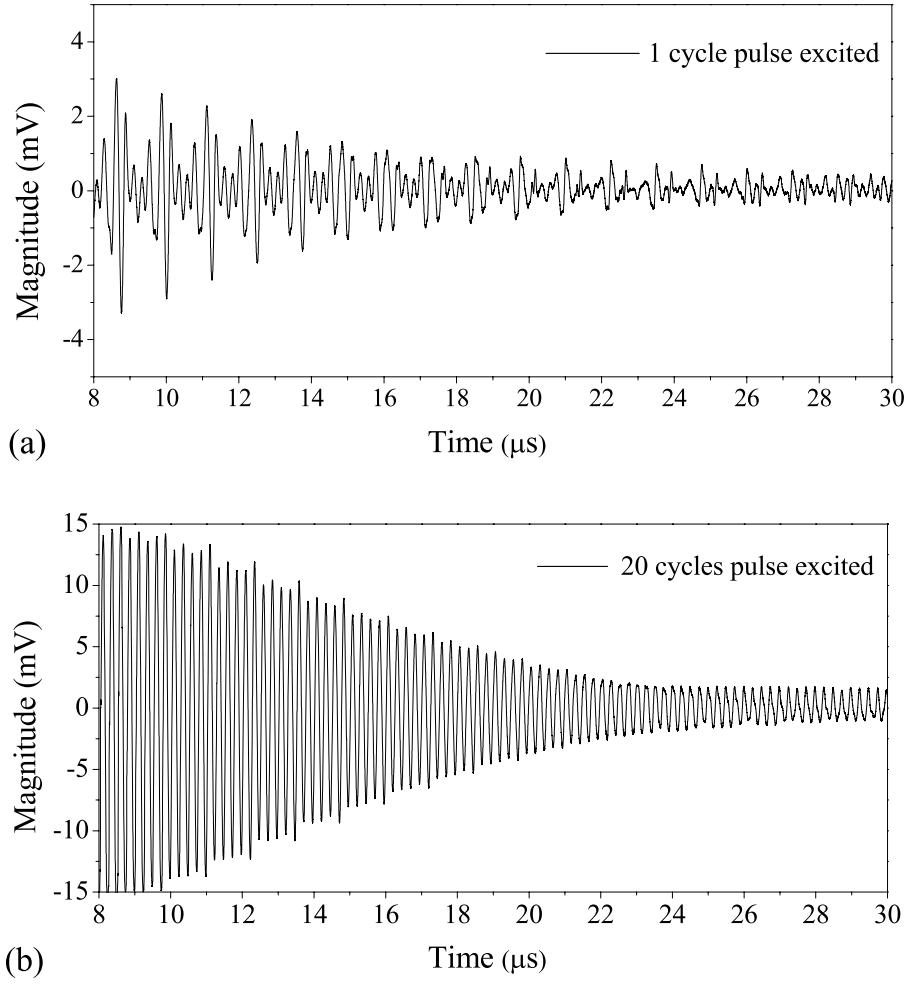

Fig. 3. Time-domain signal in a 2 mm-thickness aluminum plate with (a) 1 cycle (b) 20 cycles pulse excited.

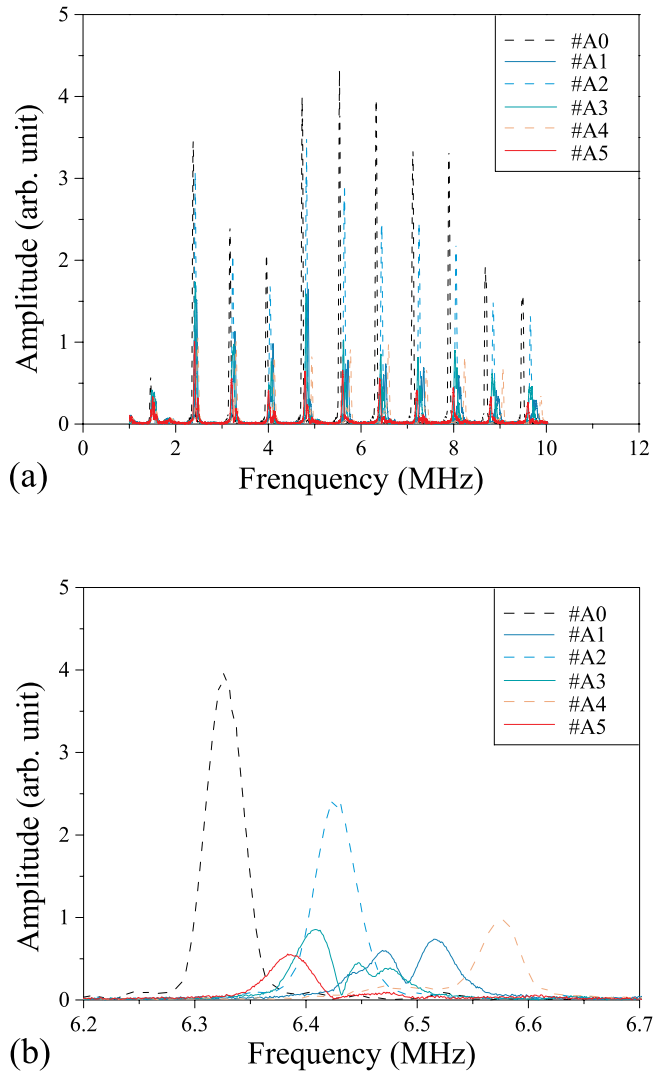

Fig. 4. Resonance frequency spectra of aluminum plates, (a) range from 1.0 to 10 MHz, (b) from 6.2 to 6.7 MHz.

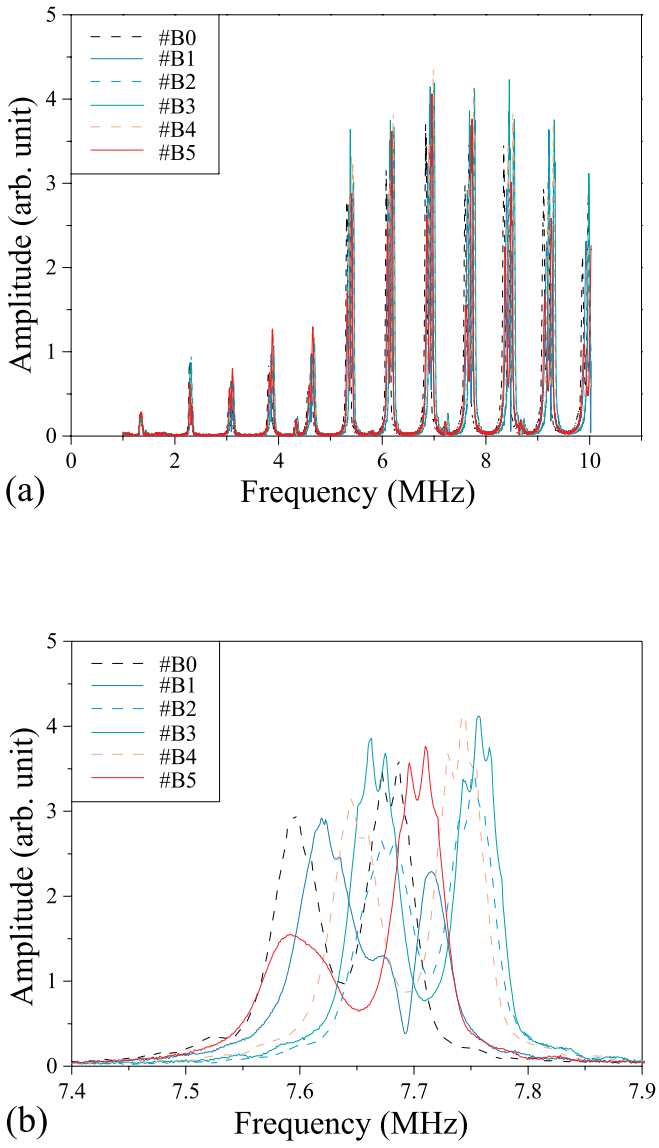

Fig. 5. Resonance frequency spectra of nickel plates, (a) range from 1.0 to 10 MHz, (b) from 7.4 to 7.9 MHz.

of six nickel plates are also obtained.

Based on Eq. (5), the shear wave velocity c_s of the tested specimens can be calculated as [19].

$$c_s = \frac{\sum_{j=m}^{n} \frac{2df_j}{j}}{m - n + 1} \tag{6}$$

where j denotes the order of a resonance frequency, m and n denote the order range of the resonance frequencies contained in the above resonance frequency spectra. Figs. 6(a) and 7(a) show the variations of shear wave velocities in different aluminum and nickel plates, it can be concluded that the shear wave velocity measured by the linear EMAR approach is not sufficiently sensitive for the assessment of thermal damage in tested plates. Furthermore, Figs. 4(b) and 5(b) indicates that the resonance frequency of the aluminum and nickel plate changed irregularly when subjected to the different thermal loadings. This phenomenon can be attributed to the thickness difference and the distinction of the thermal damage state among the specimens. As noted before, the experiments in this investigation are not related to in-situ testing of one identical sample, therefore, the shift of the resonance frequency in metallic plate cannot be well utilized for the resonance ultrasound spectroscopy as mentioned previously [13–16].

For the measurement of ultrasonic attenuation, a parameter in terms of the total amplitude of the resonance peaks (TARP) in the measured EMAR spectrum was introduced and calculated to index the shear wave attenuation. Generally, the time-domain signal of a specimen under resonant condition may not be processed as readily and precisely as the frequency spectrum with decent filters, to indicate the magnitude of the ultrasonic response in the material. In addition, a single amplitude at the resonance frequency can be influenced by the driving frequency of the EMAT and other factors. Thus, the TARP parameter involving all the frequency dependency information of the material and transducers could be used to demonstrate the attenuation of the samples in an improved reliable manner. As one can see from Fig. 6(b), the TARP parameters in the specimen decrease by 80% after thermal loading, except for the sample #A1 heated for 10 min.

The above experimental procedures were also applied to the nickel plates. Similar shear wave velocity and the TARP calculation containing only the right sides of the resonance peaks were conducted. As presented in Fig. 7(a), the shear wave velocity of the nickel plate seems to decrease first by about 3%, and then increase by about 1%, with the heating time. As for the TARP related to the material attenuation, the maximum amplitude of oscillation is about 20% with no regular patterns in regard to the heating time found in Fig. 7(b). It is important to note that each of the theoretically predicted resonance frequency peak of nickel plates

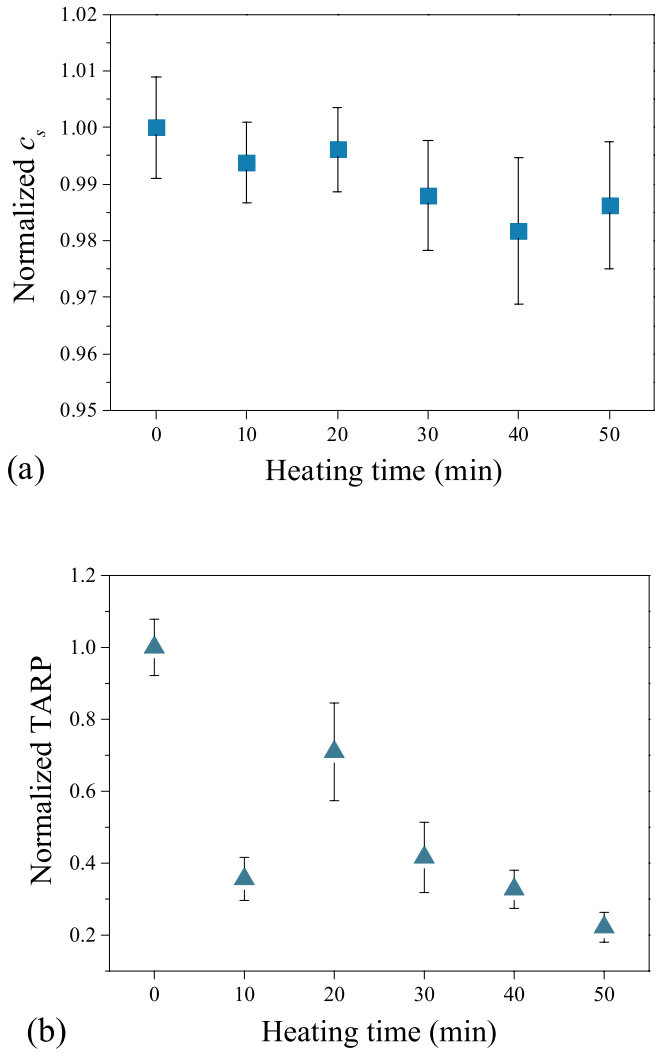

Fig. 6. Calculated linear ultrasonic parameters in aluminum plates subjected to different heating times, (a) shear wave velocity normalized by the reference raw material with $c = 2.99$km/s, (b) value of total amplitude of resonance peaks normalized by the reference raw material with $TARP = 29.34$.

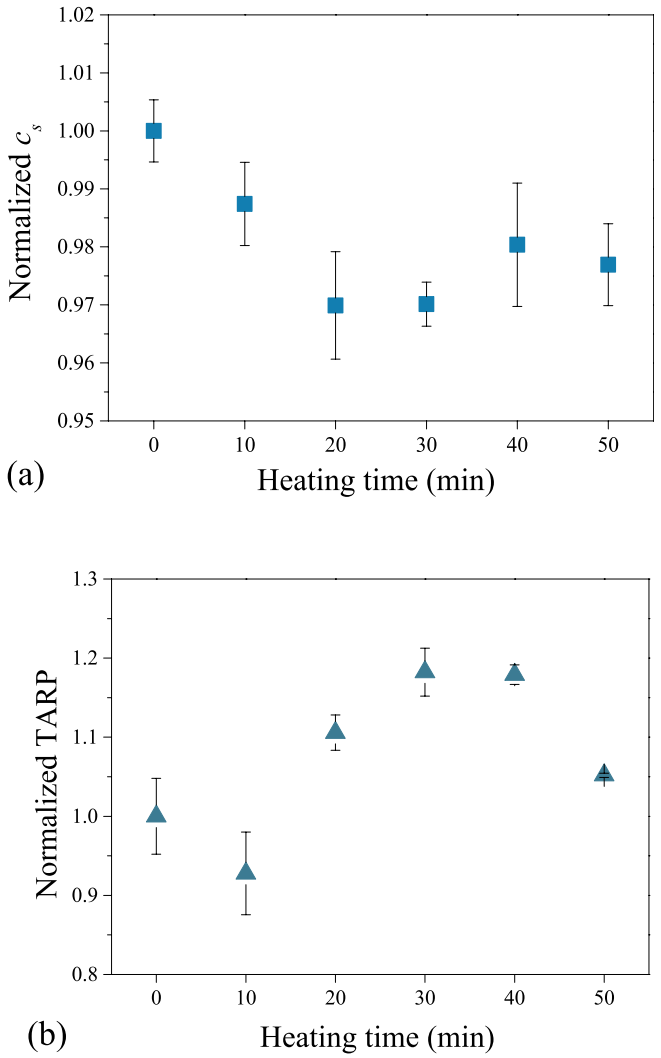

Fig. 7. Calculated linear ultrasonic parameters in nickel plates subjected to different heating times, (a) shear wave velocity normalized by the reference raw material with $c_s = 3.38$km/s, (b) value of total amplitude of resonance peaks normalized by the reference raw material with $TARP = 23.09$.

splits into two peaks, as shown in Fig. 5(b), which can be attributed to the relatively higher anisotropy of the nickel material picked up by the radial shear wave EMAT than that of the aluminum plates. Overall, even the variations of shear wave velocity and attenuation measured by linear EMAR approaches in specimens after heat treatment can be obtained by these procedures, while neither of them shows remarkable and stable trend in accordance with the heating times of the specimens, which suggests that the linear acoustic features (c_s and TARP) measured by the EMAR technique are not feasible and reliable indictors for the thermal damages in these two types of metals.

4.2. Nonlinear EMAR measurements

For nonlinear EMAR measurement, the two-step procedure was implemented as illustrated in Section 2.2. The frequency of 6.44 MHz was chosen to be the resonant frequency f_r for the aluminum plates, thereby the measured amplitude at 6.44 MHz in the frequency domain of the received signal was defined as A_1. Keeping the input power unchanged, a series of ultrasonic pulses at exciting frequency of $f_r/3$ were brought into the sample to obtain the measured signal amplitude A_3 at the resonant frequency f_r in the spectrum. It is important to note that the driving frequency of the second step did not satisfy the resonance

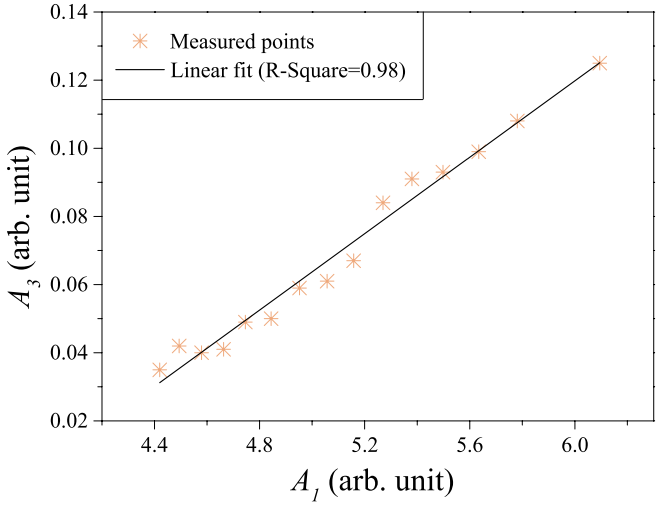

Fig. 8. Measured relationship between the amplitude of third harmonic (A_3) and that of primary wave (A_1) in aluminum plate #A0 using EMAR method.

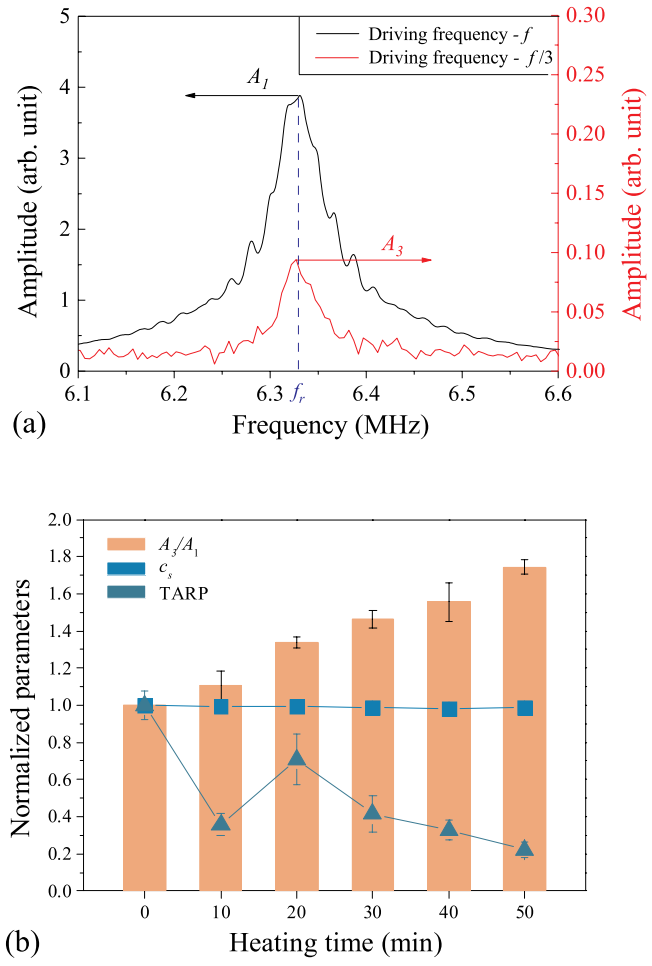

Fig. 9. Cubic nonlinearity measured in aluminum plates by EMAR method, (a) amplitudes of third harmonic and primary wave measured in specimen #A0, (b) comparison of the sensitivity of cubic nonlinearity and linear parameters to thermal damage in specimens. The acoustic nonlinearity, wave velocity and TARP are normalized by the reference raw material with ($A_3/A_1 = 0.015$), ($c_s = 2.99$ km/s), ($TARP = 29.34$).

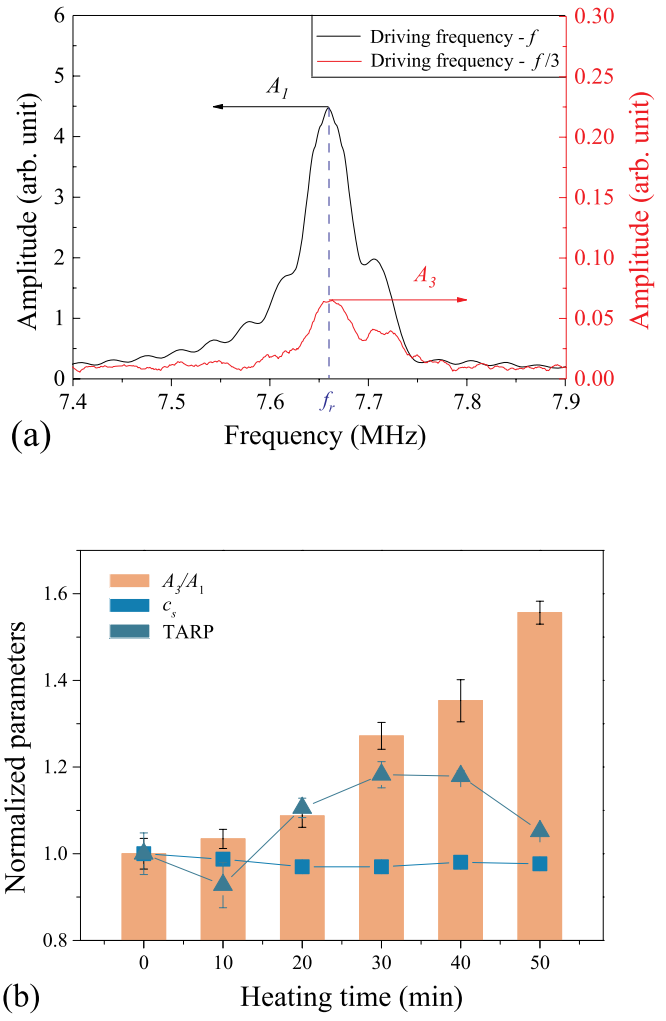

Fig. 10. Cubic nonlinearity measured in nickel plates by EMAR method, (a) amplitudes of third harmonic and primary wave measured in specimen #B0, (b) comparison of the sensitivity of cubic nonlinearity and linear parameters to thermal damage in specimens. The acoustic nonlinearity, wave velocity and TARP are normalized by the reference raw material with ($A_3/A_1 = 0.014$), ($c_s = 3.38$ km/s), ($TARP = 23.08$).

condition, making the primary shear wave at frequency of $f_r/3$ unmeasurable. While its third harmonic at triple frequency f_r satisfies the resonant condition, the received signal contains a third harmonic component. Normalization of the measured third-harmonic amplitude (A_3/A_1) is taken as the nonlinear indictor of the nonlinear EMAR technique. It is critical to verify the feasibility and validity of the proposed nonlinear indicator by checking the relationship between A_3 and A_1. Measurements were performed with increasing input gain value at the determined experimental setup. As shown in Fig. 8, a linear correlation is found between the signal amplitudes A_3 and A_1, which confirms that the parameter is stable for the nonlinear EMAR technique. Fig. 9(a) shows the amplitudes of primary and third harmonic waves in the frequency domain, and Fig. 9(b) shows the calculated normalized third-harmonic amplitudes in different samples, along with the linear ones. The data has been normalized for sensitivity comparison. As shown in Fig. 9(b), the normalized third-harmonic amplitude increases monotonously by nearly 80% with the heating time for the aluminum plates.

The resonance frequency f_r chosen for the nickel plates was around 7.66 MHz, and the experimental results are provided in Fig. 10. A similar tendency in the nickel plates can also be observed as shown in Fig. 10(b), in which 60% variation of the normalized third-harmonic amplitude is found. As demonstrated earlier, the interactions of primary shear waves with material nonlinearity will generate the third harmonics at the triple frequency. Third harmonic component of triple frequency at resonant condition is measurable using EMAR technique. It has been well accepted that higher harmonic generation could be attributed to microstructural defects such as lattice deformation or dislocation motion [42–45]. Any thermal process that alters the local atomic potential or influences the movement of dislocations will change the microstructure and the efficiency of higher harmonic generation in the specimen. Compared with the variations of measured linear acoustic features (c_s and TARP), the normalized third-harmonic amplitude, measured by the nonlinear EMAR technique proposed in this investigation, shows a reliable and sensitive potential to characterize the thermal damage in both ferromagnetic and non-ferromagnetic metals.

Noted that the EMAR method is very sensitive to the thickness of the specimen, variation of specimen thickness will cause the shift of resonance frequency of tested specimen. Meanwhile, the unstable electric voltage, as well as the surface flatness can also affect the measured amplitude of resonance frequency. By carefully polishing the surfaces of the specimens to a reasonable extent and keeping the experimental conditions consistent during the measurements, the results obtained for in-situ testing are credible with little interference from that kind of factors.

5. Conclusion

In this paper, a nonlinear EMAR technique was proposed for assessment of thermal damage in aluminum and nickel plates, which combines the advantage of EMAR with that of the higher harmonic generation. EMAR technique makes up the low energy transition efficiency of the EMATs and enhances the SNR. Non-contact experimental setup ensures the consistency of coupling condition and improves the reliability of ultrasonic measurements. Experimental results indicate that the measure of third-harmonic amplitude at the resonant frequency can be a promising means for thermal damage assessment both in ferromagnetic and non-ferromagnetic materials. The comparison of linear and nonlinear EMAR techniques shows that the normalized third-harmonic amplitude measured by the EMAR technique is a more stable and sensitive indicator for thermal damage characterization. The developed non-contact experimental scheme in this investigation can be extended to a cost-effective in situ measuring apparatus for monitoring material degradation.

Acknowledgement

This research was funded by the National Natural Science Foundation of China, grant number 11774295, 11834008, 11474361 and 11274388.

References

[1] Tamura A, Zhong C, Croxford AJ, Wilcox PD. A feasibility study of noncontact ultrasonic sensor for nuclear power plant inspection. J Nucl Eng Radiat Sci 2017;3(2):021003.
[2] Ohtani T, Ogi H, Hirao M. Noncontact evaluation of surface-wave nonlinearity for creep damage in Cr-Mo-V Steel. Jpn J Appl Phys 2009;48(7). 07GD02-07GD02-6.
[3] Choi S, Cho H, Lindsey MS, Lissenden CJ. Electromagnetic acoustic transducers for robotic nondestructive inspection in harsh environments. Sensors 2018;18(1):193.
[4] Hernandezvalle F, Dixon S. Pulsed electromagnet EMAT for ultrasonic measurements at elevated temperatures. Insight - Non-Destructive. Test. Cond. Monit 2011;53(2):96–9.
[5] Kaczmarek M, Piwakowski B, Drelich R. Noncontact ultrasonic nondestructive techniques: state of the art and their use in civil engineering. J Infrastruct Syst 2016;23(1):B4016003.
[6] Jr RG. Non-contact ultrasonic techniques. Ultrasonics 2004;42(1):9–16.
[7] Hirao M, Ogi H. Electromagnetic acoustic transducers: noncontacting ultrasonic measurements using EMATs. second ed. Springer Japan; 2017.
[8] Jeong K, Lee J, Kim T, Cho Y. Aircraft component defect monitoring by the use of patch magnetostrictive EMAT. J Vis 2017;20(4):847–58.
[9] Thring CB, Fan Y, Edwards RS. Focused Rayleigh wave EMAT for characterisation of surface-breaking defects. NDT E Int 2016;81:20–7.
[10] Kang L, Zhang C, Dixon S, Zhao H, Hill S, Liu M. Enhancement of ultrasonic signal using a new design of Rayleigh-wave electromagnetic acoustic transducer. NDT E Int 2016;86:36–43.
[11] Benegal R, Karimi F, Filleter T, Sinclair AN. Optimization of periodic permanent magnet configuration in Lorentz-force EMATs. Res Nondestruct Eval 2016;(12):95–108.
[12] He J, Xu K, Ren W. Designs for improving electromagnetic acoustic transducers' excitation performance. Jpn J Appl Phys 2018;57(6):067202.
[13] Abeele EAVD, Carmeliet J, Cate JAT, et al. Nonlinear elastic wave spectroscopy (NEWS) techniques to discern material damage, Part II: single-Mode Nonlinear Resonance Acoustic Spectroscopy. Res Nondestruct Eval 2000;12(1):31–42.
[14] Johnson PA, Zinszner B, Rasolofosaon PNJ. Resonance and elastic nonlinear phenomena in rock. J Geophys Res 1996;101(B5):11553.
[15] Maier S, Kim JY, Forstenh UM, et al. Noncontact nonlinear resonance ultrasound spectroscopy (NRUS) for small metallic specimens. NDT & E International; 2018. S0963869517305911.
[16] Sylvain H, Guerard S, Fran P, et al. Nondestructive characterization of cortical bone micro-damage by nonlinear resonant ultrasound spectroscopy. PLoS One 2014;9(1):e83599.
[17] Kawashima K, Wright OB. Resonant electromagnetic excitation and detection of ultrasonic waves in thin sheets. J Appl Phys 1992;72(10):4830–9.
[18] Hirao M, Ogi H. Electromagnetically excited acoustic resonance for evaluating attenuation coefficient and grain size in polycrystalline metals. Appl Phys Lett 1994;64(17):2217–9.
[19] Wang B, Wang X, Hua L, Li J, Xiang Q. Mean grain size detection of DP590 steel plate using a corrected method with electromagnetic acoustic resonance. Ultrasonics 2017;76:208–16.
[20] Hirao M, Ogi H. Electromagnetic acoustic resonance and materials characterization. Ultrasonics 1997;35(6):413–21.
[21] Jhang KY. Nonlinear ultrasonic techniques for nondestructive assessment of micro damage in material: a review. Int J Precis Eng Manuf 2009;10(1):123–35.
[22] Klepka A, Staszewski WJ, Jenal RB, Szwedo M, Iwaniec J, Uhl T. Nonlinear acoustics for fatigue crack detection – experimental investigations of vibro-acoustic wave modulations. Structural Health Monitoring. Int J 2012;11(2):197–211.
[23] Aymerich F, Staszewski WJ. Impact damage detection in composite laminates using nonlinear acoustics. Compos Appl Sci Manuf 2010;41(9):1084–92.
[24] Cobb WN. Finite amplitude method for the determination of the acoustic nonlinearity parameter B/A. J Acoust Soc Am 1983;73(5):1525–31.
[25] Ostrovsky LA. Wave processes in media with strong acoustic nonlinearity. J Acoust Soc Am 1991;90(6):3332–7.
[26] Donskoy D, Sutin A, Ekimov A. Nonlinear acoustic interaction on contact interfaces and its use for nondestructive testing. NDT E Int 2001;34(4):231–8.
[27] Kim JY, Jacobs LJ, Qu JM. Experimental characterization of fatigue damage in a nickel-base superalloy using nonlinear ultrasonic waves. J Acoust Soc Am 2006;120(3):1266–73.
[28] Walker SV, Kim JY, Qu J, Jacobs LJ. Fatigue damage evaluation in A36 steel using nonlinear Rayleigh surface waves. NDT E Int 2012;48:10–5.
[29] Li W, Cho Y, Achenbach JD. Detection of thermal fatigue in composites by second harmonic Lamb waves. Smart Mater Struct 2012;21:085019.
[30] Li W, Cho Y. Thermal fatigue damage assessment in an isotropic pipe using nonlinear ultrasonic guided waves. Exp Mech 2014;54(8):1309–18.
[31] Li W, Lee J, Achenbach JD. Assessment of heat treated inconel X-750 alloy by nonlinear ultrasonics. Exp Mech 2013;53(5):775–81.
[32] Sun L, Kulkarni SS, Achenbach JD, Krishnaswamy S. Technique to minimize couplant-effect in acoustic nonlinearity measurements. J Acoust Soc Am 2006;120(5):2500–14.
[33] Operation manual, model SNAP-0.25-7, ritec advanced measurement system. Ritec Inc.; 2002.
[34] Deng MX, Wang P, Lv XF. Experimental observation of cumulative second-harmonic generation of Lamb-wave propagation in an elastic plate. J Phys D Appl Phys 2005;38(2):344–53.
[35] Hiro M, Ogi H. EMATs sonic measurements. Massachusetts: Kluwer Academic Publishers; 2003.
[36] Wochner MS, Hamilton MF, Ilinskii YA, Zabolotskaya EA. Cubic nonlinearity in shear wave beams with different polarizations. J Acoust Soc Am 2008;123(5):2488–95.
[37] Hamilton MF, Blackstock DT. Nonlinear acoustics. San Diego: Academic Press; 1998. p. 263–77.
[38] Zhu Q, Chen M, Ban C, et al. Effect of annealing temperature on deformed microstructure of high purity aluminum. Heat Treat Met 2011;36(6):111–4.
[39] Li N, Ye S. Effect of homogenization annealing on microstructure and properties of high purity aluminum foil. Light Met 1993;(9):50–4.
[40] Lee TR, Chang CP, Kao PW. The tensile behaviour and deformation microstructure of cryo-rolled and annealed pure nickel. Mater Sci Eng A 2005;408(1–2):131–5.
[41] Welsh SL, Monica K, Underwood OD, et al. Influence of grain boundary character and annealing time on segregation in commercially pure nickel. J Mater 2016;2016:1–15.
[42] Ogi H, Hirao M, Honda T. Ultrasonic attenuation and grain-size evaluation using electromagnetic acoustic resonance. J Acoust Soc Am 1995;98:458–64.
[43] Cantrell JH. Substructural organization, dislocation plasticity and harmonic generation in cyclically stressed wavy slip metals. Proc. R. Soc. A 2004;A460:757–80.
[44] Kim JY, Qu J, Jacobs LJ, Littles JW, Savage MF. Acoustic nonlinearity parameter due to micro-plasticity. J Nondestruct Eval 2006;25(1):28–36.
[45] Ogi H, Hirao M, Aoki S. Noncontact monitoring of surface-wave nonlinearity for predicting the remain life of fatigue steels. J Appl Phys 2001;90(1):438–42.